ce/papers Proceedings in civil engineering

Ernst & Sohn A Wiley Brand

ORIGINAL ARTICLE

eurosteel AMSTERDAM 2023

Ernst & Sohn A Wiley Brand

Robot supported Wire Arc Additive Manufacturing of Steel Columns

Benedikt Waldschmitt[1] | Jörg Lange[1]

Correspondence

Benedikt Waldschmitt, M.Sc.
Technical University of Darmstadt
Institute for Steel Construction
and Materials Mechanics
Franziska-Braun-Straße 3
64287 Darmstadt
Email: waldschmitt@stahlbau.tu-darmstadt.de

[1] Technical University of Darmstadt, Darmstadt, Germany

Abstract

Wire Arc Additive Manufacturing (WAAM) is a robot-controlled welding process used to build up three-dimensional structures in steel. Like other Additive Manufacturing (AM) technologies, WAAM allows for geometrically-complex structures to be manufactured which may be unfeasible using conventional methods. Over recent years, WAAM has also gained prominence in the fields of architecture and civil engineering, with applications ranging from fully-printed steel bridges to individualized steel components. This paper presents the additive manufacturing process of large-scale applications, focusing on steel columns with circular hollow cross-sections (CHS). The paper highlights the specific features of the necessary welding and process parameters before the manufacturing process is described in detail. Digital models and welding trajectories are generated with Parametric Robot Programming (PRP) and serve the robot-controlled printing process. The AM itself is monitored by multiple process-control checks giving information about resulting weld thicknesses, heights and welding errors influencing the manufacturing strategy of the CHS columns. To be able to make a closing statement about the load-bearing capacity of the WAAM-manufactured CHS, final load tests on (stub) columns are carried out.

Keywords

WAAM, Additive Manufacturing, Parametric Robot Programming, Steel column, CHS, stub column

1 Introduction

Today many buildings not only have to serve functional requirements but also have representative purposes. Their construction and design calls for a non-standardized approach, making use of highly individualized structures in addition to standard elements. To connect standard elements with each other, steel connections (e.g., flag plate connections or head plates) have been optimized for the conventional manufacturing processes. Although today's steel fabricators are already able to produce rather individualized structures and connections (shown in Figure 1) the manufacturing process is still very elaborate, expensive, and time-consuming. In addition, an increased shortage of skilled workers argues for greater automation. In a first approach fully automated I-beam production lines were implemented which are only used by specialized steel fabrication companies worldwide. In these systems, handling robots hold plates (stiffeners, base and head plates, etc.), while welding robots weld the seams (Figure 2). This is not feasible for more complex geometries, such as Y-shaped columns. Figure 1 visualizes a three-dimensional model of a Y-shaped complex steel structure, multiple

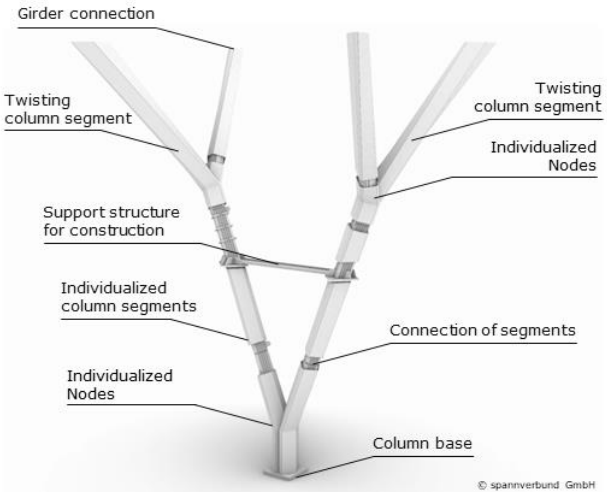

Figure 1 Y-shaped steel structure made by combining individualized steel nodes and column segments

times manufactured by spannverbund GmbH. It combines straight and twisted column segments by individualized

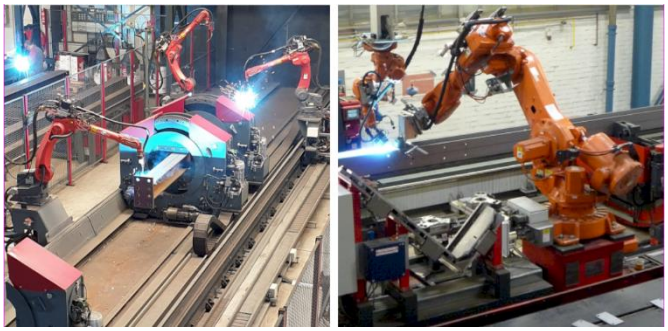

Figure 2 Automated production line with three welding robots (left) and one welding- and one handling robot (right)

nodes. Although Additive Manufacturing (AM) has not yet been fully established in the steel construction industry, it shows the potential in terms of individualization and automation for different applications [1]. It provides a high variety of utilizations which could improve constructions. This article will present the manufacturing of various CHS columns using an already developed design-to-manufacturing workflow. Based on measured layer information and collected welding and process data, an evaluation of the production is performed. Finally, the load-bearing capacity of several structures under compressive loading will be analysed.

2 Wire Arc Additive Manufacturing

Within the steel construction industry, the research in Wire Arc Additive Manufacturing (WAAM) has raised attention. WAAM is an additive manufacturing process based on gas shielded metal arc welding (GMAW). The electric arc (mostly short arc and spray arc) melts the welding wire which serves as the printing material. The liquid molten pool solidifies in lines or spots and forms three-dimensional structures. The shielding gas protects the material deposition from atmospheric influences and impurities. At the same time, it stabilizes the heat input of the welding process and influences the molten pool [2]. The degree of viscosity, the length and kind of active and passive cooling and thus the solidification process are decisive for the geometric shape of the seam and the target geometry. The selection of the wire electrode significantly determines the material characteristics of the manufactured structure. Six-axis robotic systems, like the one at the laboratory of TU Darmstadt, given in Figure 3, for guiding the welding torch offer great flexibility in the manufacturing of components and are used to ensure production in large installation spaces. With increasing size, accuracy decreases as

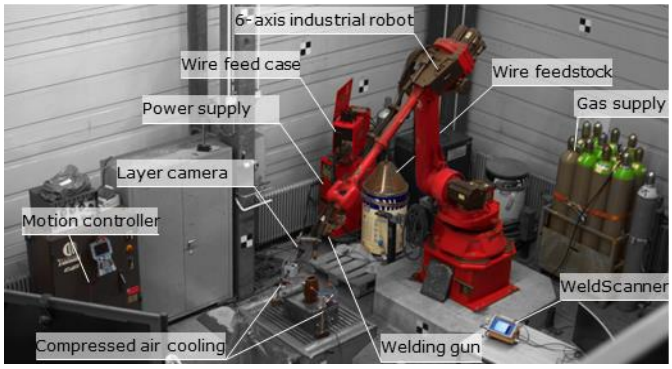

Figure 3 Six-axis robotic system for Wire Arc Additive Manufacturing at the laboratory at TU Darmstadt, manufacturing a column structure

the distance to the machine origin extends [3]. To avoid inaccuracies large structures might be divided in segments to be manufactured simultaneously. At the same time, WAAM offers higher deposition rates compared to other metallic additive manufacturing processes and investment costs for supplies and system technology are significantly lower [4]. These aspects make the process attractive for the production of large structural components like free form columns and its single components.

3 WAAM as a tool for manufacturing steel columns

Through the widespread availability of digital design tools architects have been enabled to design ever more unusual structures. This is particularly evident in the context of additive manufacturing. Standardized load-bearing column elements can be redesigned into geometrically complex and structurally efficient elements. Researchers at the University of Bologna worked with MX3D to illustrate the possibilities of combining digital design tools with additive manufacturing by producing large-scale, lattice-like columns [5]. In addition to geometric optimization of cross sections, the topic of stability is becoming the focus of current research in WAAM-manufactured elements. Initial investigations at the TU Darmstadt [6] and recent studies at Imperial College provide the first indications of component behaviour for slender components at risk of flexural buckling under compressive loading [7].

4 Design-to-manufacturing workflow

A design-to-manufacturing workflow has been established at TU Darmstadt to additively manufacture individual columns (components) by means of WAAM. Detailed information can be found in [8]. A digital model serves to generate welding trajectories. The coordinates on the circular path of the CHS are determined using Parametric Robot Programming (PRP), a coordinate determination based on mathematical functions. These functions contain information about the circle radius as well as the structure and layer heights, so that a dynamic adjustment of the coordinates can be implemented to avoid errors in the geometry development and to ensure a stable manufacturing process. Following the manufacturing itself collected data (welding data, geometric and process information) is evaluated and stored to a rudimentary digital twin which could be complimented by additional information of a target/actual-comparison or life cycle data.

5 Process and input parameters

Material deposition in a stable welding process depends largely on the selected welding and input parameters. Both significantly influence the geometric dimensions of a weld and the subsequent material properties. The process is decisively controlled by the wire feed speed, the defined travel speed of the robot and the CMT (Cold Metal Transfer) process regulation, an energy reduced welding process provided by Fronius. Table 1 lists the welding parameters for a Fronius CMT Advanced 4000 R welding source with a CMT Cycle Step characteristic – which if set right offers a precise control of the material deposition - and relevant process parameters. To prevent the weld metal from dripping, active (WAC) and passive (NC) cooling periods are set for structures after each layer so the upper

edges can cool down. Preliminary investigation showed an expected layer height of 1.35 mm and a wall thickness of 4.5 mm for vertical printing.

Table 1 Process and input parameters

Process and input parameter	Variable	Unit
Number of CMT-Cycles	15 – 25	-
Pause time	100	ms
Wire-Feed-Speed (set)	6.0	m/min
Travel-Speed	0.6	m/min
Gas-set	15	l/min
Wire electrode	Weko 2 G3Si1 (ER 70S-6) Ø 1.2 mm	
Shielding Gas	Ferroline C6X1 (93 % Argon, 6 % CO_2, 1 % O_2)	
Welding torch orientation	90° to the horizontal	
Cooling	WAC	Water + Air pressure cooling
	NC	None active cooling

6 Additive manufacturing of Circular Hollow Sections

For the manufacture of the CHS columns of different element heights, exemplarily shown in Figure 4 and listed in Table 2, two manufacturing strategies were followed. The outer diameter of all CHS is ≈ 60.3 mm with the intended wall thickness of 4.5 mm. Column CHS_500_1 was manufactured individually, all other columns in a serial manufacturing approach. Figure 5 shows the manufacturing strategy for the remaining columns CHS_40_1 - 3, CHS_470_1 -3 and CHS_1000_1 - 3. The recalculated coordinates of each layer are used to deposit the material per structure. Subsequently to stabilize the process, the active or passive cooling phase starts for each column with the aim of reducing the interlayer temperature to below 150 °C before a new layer is processed. Every 10 layers, the wall thickness and the interlayer temperature are recorded before finishing the next layer. Depending on the workpiece, this process is supplemented every 20 - 40 layers by a tactile measurement (TouchSense) of the current workpiece height to examine the layer height and make any necessary adjustments. This procedure has already proven successful in the manufacturing of more complex column geometries in shorter layer intervals [8]. In addition, the welding data is recorded for each layer and a layer image is created for each structure.

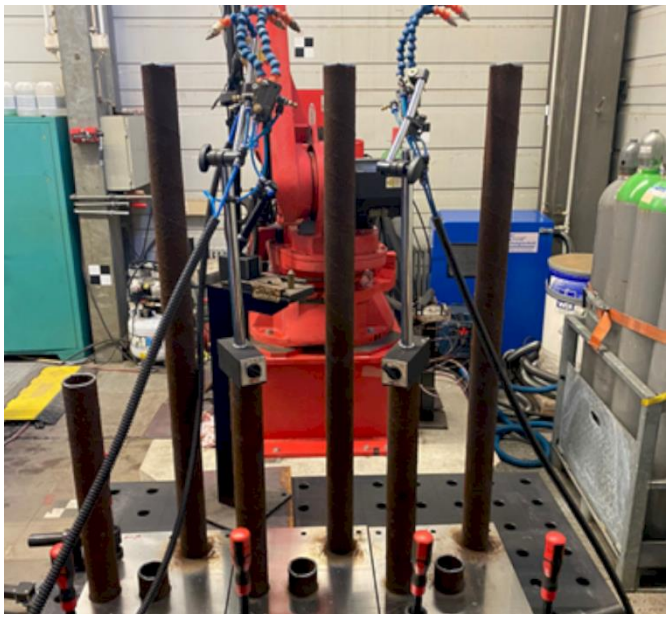

Figure 4 Serial additive manufacturing of CHS columns of different structural heights

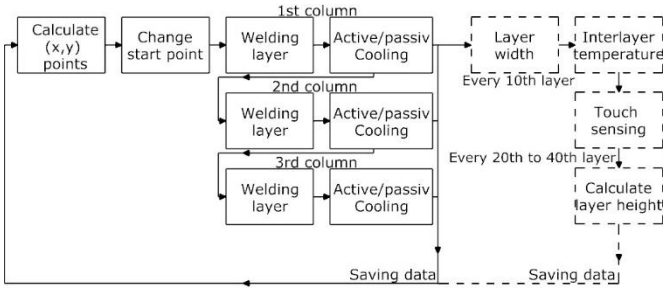

Figure 5 Manufacturing strategy for CHS-columns per each layer

7 Evaluation of the AM process

7.1 Geometric shape

Except for CHS_500_1 (deviation of approx. 8%), the manufactured CHS show a high degree of correspondence to the predicted geometric dimensions, in particular the layer heights. Figure 6 (left) illustrates the measured information about the layer hight and width for different structures measured following the described principal above. A total of 5230 layers were manufactured for the different test specimens. The frequently measured layer widths represent the maximum extension of the weld bead. Higher deviations result from manual measuring of the 8 measuring points per layer. The resulting cross-sectional areas therefore overestimate the cross-section, which is why a minimum cross-sectional area of 7.89 cm² is assumed for the subsequent examination of the structural analysis. An examination of the interlayer temperature Figure 6 (right), which was recorded at specific spots, shows that the limit value of 150 °C was largely kept by active and passive cooling phases. For CHS_500_1, this is around 100 °C. Nevertheless, the higher layer width and lower layer height indicate an overall higher interlayer temperature during manufacturing. The reason for this is assumed to be the reduced cooling phase (despite maximum cooling capacity). Since the temperature was only recorded every 10 layers, it may be higher during the manufacturing interval and thus favor widening of the layer. For future investigations, a thermal image camera is to be installed during and after the welding process for a more precise recording.

Table 2 Overview of measured characteristics of the manufactured CHS elements and corresponding recorded welding/process errors

Structure	General information					Cross-section		Welding/process errors				
	Layers	Active cooling	Structure Height H_{total} in mm	Layer Height h in mm	Outer Diameter D in mm	Wall thickness $t_{measured}$ in mm	Area A in cm²	Ignition failure	Welding Interup-tion	Burn-back failure	Pores	Wire stick
CHS_1000_1		WAC						1	21	3	7	16
CHS_1000_2	762	WAC	1019.9	1.349 ± 0.012	6.03	4.591 ±0.146	8.034	4	22	2	9	10
CHS_1000_3		WAC						6	25	4	1	10
CHS_500_1	400	WAC	492.0	1.240 ± 0.006	6.03	4.81 ± 0.221	8.392	2	13	5	1	5
CHS_450_1		WAC						1	7	1	0	5
CHS_450_2	340	WAC	454.5	1.335 ± 0.057	6.03	4.624 ±0.185	8.392	0	10	1	0	11
CHS_450_3		NC						0	5	0	4	8
CHS_470_1		WAC						5	19	9	4	9
CHS_470_2	362	WAC	469.6	1.293 ± 0.018	6.03	4.589 ±0.133	8.031	1	8	7	4	11
CHS_470_3		NC						3	7	5	2	8
CHS_140_1		NC						0	4	3	1	0
CHS_140_2	107	NC	141.0	1.361 ± 0.067	6.03	4.766 ±0.089	8.314	0	4	2	1	0
CHS_140_3		NC						0	4	4	0	0
CHS_40_1		NC						0	1	0	2	1
CHS_40_2	39	NC	54.0	1.360 ± 0.077	6.03	4.554 ±0.091	7.975	0	2	0	0	2
CHS_40_3		NC						0	0	0	1	2
Total	5230			1.33 ± 0.03	6.03	4.62 ± 0.15	8.09	23	152	46	37	98
								0.44%	2.91%	0.88%	0.71%	1.87%
Total*	4830			1.34 ± 0.03	6.03	4.61 ± 0.15	8.06	21	139	41	36	93
* without Column CHS_500_1								0.43%	2.88%	0.85%	0.75%	1.93%

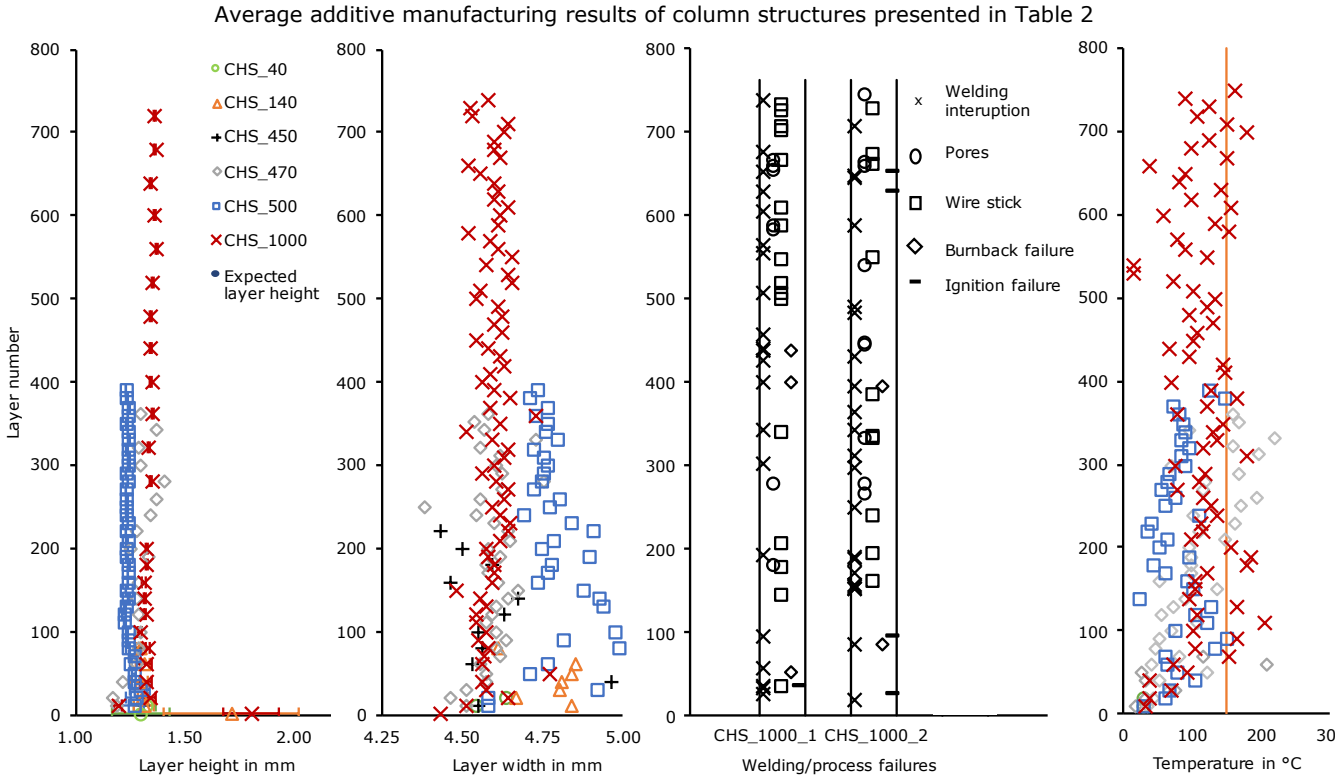

Figure 6 Illustration of frequently recorded data while manufacturing the CHS; average layer height (left); average layer width (mid-left); welding failures (mid-right); and average interlayer temperature of the upper layers (right)

7.2 Welding errors

Each layer welding data was recorded with a WeldScanner P1000 DV 25 GAS30l10b Version 4.2 from the company HKS-Prozesstechnik GmbH using a scanning rate of 100 Hz. During manufacture, welding/process errors occurred at irregular intervals, e.g., due to errors during the ignition of the arc or the burnback of the wire at the end of a seam. Each time, a visual inspection was performed to ensure that the microstructure was not weakened by pores. In the rare cases where pores occurred, they were removed, and the resulting gap was filled manually.

Any defects that occurred were noted in a logbook and after completion of manufacturing, the welding data of the corresponding layers were randomly examined. This

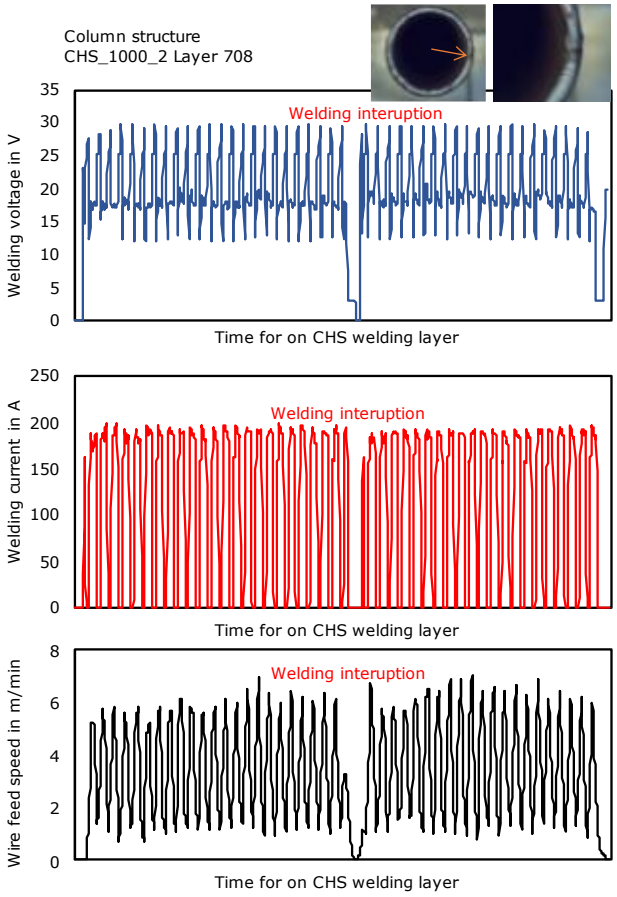

Figure 7 Exemplary illustration of the weld data recording with a recognizable weld failure - weld interruption during the manufacturing of the 708th layer of the column CHS_1000_2

revealed recurring error patterns - exemplified by a welding interruption during the manufacture of layer 708 of the CHS_1000_2 shown in Figure 7. This analysis can be important for determining any wall inhomogeneities from production and for assessing the production process and any scaling. In Table 2, all recorded defects of a structure are listed according to defect type (particularly illustrated for CHS_1000_1 and 2 in (Figure 6). It shows that defects occur in about 7 % of all layers. Half of these errors are process failures such as ignition errors, burnback failures or wire stick, which have no direct influence on the material deposition but can be a particularly relevant criterion from an economic point of view. For an analysis of the load-bearing capacity and the detection of structural defects, an accurate detection of welding interruptions and pores is crucial. While welding interruptions show a clear pattern, this could not be identified for the appearance of pores. In addition to the influence of the shielding gas dome by the torch-side suction and turbulence caused by the compressed air cooling, a higher interlayer temperature is suspected as a possible cause. Nevertheless, a precise correlation between interlayer temperature and process errors could not be observed. A more detailed investigation could be carried out using AI to determine an automated classification and location of possible imperfections and inhomogeneities in the wall thickness. Alternatively, a live evaluation in combination with a robot handling also a milling head could automatically rework the defective part and afterwards continue the manufacturing process.

8 Load-bearing capacity testing of CHS stub columns

During the testing the load-bearing capacity of four small stub columns (height ≤ 55 mm) and three more slender columns (height ≤ 432 mm) was investigated. The tests were carried out in an MAN 1000 kN hydraulic universal testing machine (UT), which is shown in Figure 8 (left and right).

Figure 8 Setup for compression testing of small stub columns (left and middle) and first approach to test slender CHS (right)

The end-platens of the testing setup were flat and parallel. The readings of load and displacement were recorded by the UT at a rate of 0.5 Hz. Additionally stereo digital correlation image equipment (DIC) recording at a rate of 1 Hz was applied to collect and log the stub columns displacement and axial strain using the software VicSnap 9. The UT was set to displacement control at a rate of 1.0 mm/min and the specimens were loaded in compression beyond the ultimate load until at least 8 mm of axial displacement (about 15%) were recorded. Table 3 lists the specific height of each specimen and their slight deviation. In addition, the determined material properties are given. To calculate the stress values a cross-section surface of 7.89 cm² was set. Figure 9 illustrates the force-displacement and the stress-strain diagram of the 7 specimens. For the stub columns, a half-sided investigation was carried out by means of DIC in the area of the buckling (Figure 8 middle). On the one hand, the surface was evaluated over the entire height of the component (FS) and, while in a second step only the area of the buckling (BA) was investigated to obtain a statement on the stress-strain behaviour. For the specimens CHS_450_D_450_1 to 3, the displacement was merely measured via the crosshead travel. Influences from the stiffness of the test setup and the UT cause an overestimation of the displacement and strain values and give only a qualitative insight. At the same time the recorded load values and resulting stresses can give an impression of the load-bearing capacity of

Table 3 Dimensions of the tested (stub) columns and resulting material properties recorded by DIC and UT

Specimen	h		$f_{y,average}$	$f_{u,average}$	E
	in mm	in mm	in kN/cm²	in kN/cm²	in kN/cm²
CHS_40_D_40_1_NC_DIC_FS	44.77	±0.057	42.82	58.46	9963.58
CHS_40_D_40_1_NC_DIC_BA			42.85	58.49	11890.41
CHS_40_D_40_2_NC_DIC_FS	44.80	±0.129	42.72	58.44	21663.98
CHS_40_D_40_2_NC_DIC-BA			43.07	58.44	23556.64
CHS_40_D_40_3_NC_DIC_FS	44.44	±0.056	41.15	57.70	17853.29
CHS_40_D_40_3_NC_DIC_BA			41.16	55.69	19177.18
CHS_500_D_40_1_WAC_DIC_FS	55.01	±0.129	39.29	63.90	23527.88
CHS_500_D_40_1_WAC_DIC_BA			39.03	59.11	18571.44
CHS_450_D_450_1_WAC_UT	428.01	-	40.95	44.60	-
CHS_450_D_450_2_WAC_UT	431.00	-	41.07	44.98	-
CHS_450_D_450_3_NC_UT	432.00	-	38.16	42.70	-

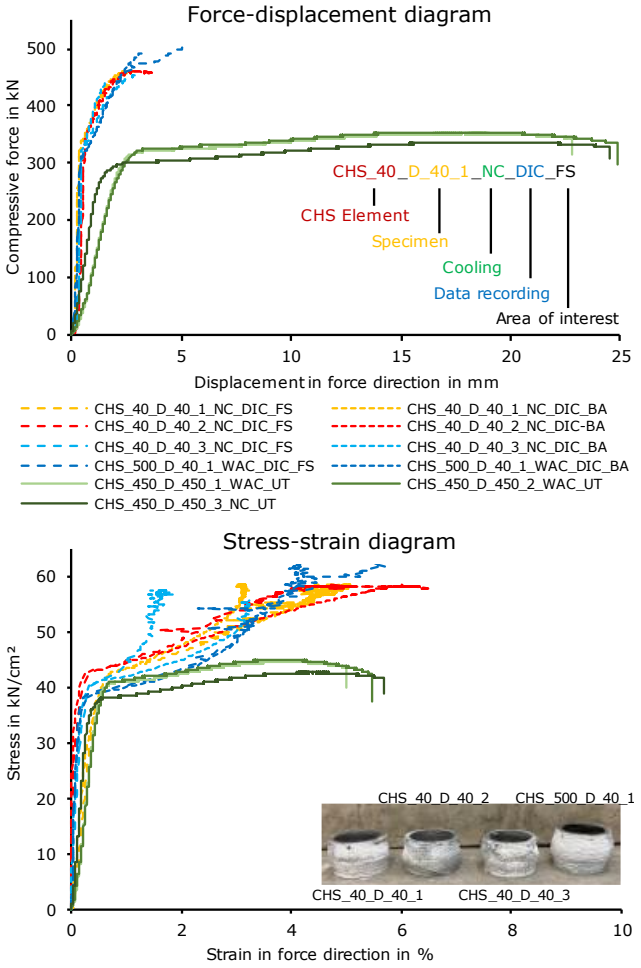

Figure 9 Force-displacement diagram and Stress-strain diagram of the investigated column structures

each element. The given DIC values are calculated by the average value of each area of interest. Therefore, a Young's modulus/tangent modulus can only be determined for the stub columns. Except for CHS_40_D_40_1, these amount between 17853 - 23527 kN/cm² in the range of 0.00 to 0.15 % strain. Due to the cracking of the primer and the speckle pattern for large deformations, the analysis of the DIC-images had to be stopped close to reaching the ultimate load. Nevertheless, it shows an indication of reduced yield strength which could be linked to high interlayer temperatures within the none actively cooled specimen CHS_450_D_450_3_NC and previous described CHS_500_D_40_1_WAC. At the same time, all stub column specimens show slightly increased tensile strength values from 55.67 up to 63.90 kN/cm² compared to the wire electrode material properties. This indicates that there is no structural defect due to pores or interruptions in the welding process. CHS_450_D_450_1 - 3 have a lower maximum load capacity. This could be due to geometric imperfections from manufacturing and a non-parallelism alignment of the end-platens in the test setup. As an attempt to provide a more profound statement, a larger number of stub column samples will be examined.

9 Conclusion

The article presented the manufacturing strategy of different CHS columns using WAAM as an approach for the future manufacturing of complex column geometries. For an evaluation of the process, data was recorded and analysed during fabrication.

- A high reproduction degree of the welding layers is shown, except for CHS_500_1.
- Welding data could be used for the identification of different welding/process errors and structural weak points.
- Initial investigations of the load-bearing capacity show component behaviour approximating the expected material properties of the wire electrode. However, influences from higher interlayer temperatures and geometric imperfections have not been considered, yet.

Nevertheless, the potential of WAAM to design individualized column elements was demonstrated in the area of manufacturing and initial component investigations.

10 Acknowledgment

We would like to thank the companies Fronius Deutschland GmbH, Messer SE & Co. KGaA, WDI – Westfälische Drahtindustrie GmbH and spannverbund GmbH for their kind support. This research was funded by the German Federal Ministry for Economic Affairs and Energy (grant number: 16KN076133).

References

[1] Buchanan, C.; Gardner, L. (2019) *Metal 3D printing in construction: A review of methods, research, applications, opportunities and challenges* in: Engineering Structures 180, S. 332–348. https://doi.org/10.1016/j.engstruct.2018.11.045

[2] Kampffmeyer, D.; Wolters, M. (2015) *Moderne Schutzgase zum MAG-Schweißen von unlegierten Stählen* in: *DVS Congress 2015*. Nürnberg. Düsseldorf: DVS Media, S. 249–253.

[3] Bandari, Y. et al. (2015) *Additive manufacture of large structures: robotic or CNC systems?* in: University of Texas at Austin [Hrsg.] *26th international solid freeform fabrication symposium*. Austin, Texas.

[4] Martina, F.; Williams, S. (2015) *Wire+arc additive manufacturing vs. traditional machining from solid: a cost comparison*. Cranfield: Cranfield University.

[5] Laghi, V. et al. (2020) *Computational design and manufacturing of a half-scaled 3D-printed stainless steel diagrid column* in: Additive Manufacturing 36, S. 101505. https://doi.org/10.1016/j.addma.2020.101505

[6] Feucht, T.; Lange, J. (2019) *3-D-printing with steel: Additive Manufacturing of Connection Elements* in: S. 419–424.

[7] Huang, C. et al. (2022) *Flexural Buckling of Wire Arc Additively Manufactured Tubular Columns* in: Journal of Structural Engineering 148, H. 9. https://doi.org/10.1061/(ASCE)ST.1943-541X.0003427

[8] Waldschmitt, B. et al. (2022) *3d printing of column structures for architectural applications* in: Architecture, Structures and Construction. https://doi.org/10.1007/s44150-022-00050-z